Title

Suppression of the motor deficit in a mucolipidosis type IV mouse model by bone marrow transplantation.

Journal

Human Molecular Genetics, 25(13)

Authors

Walker, Marquis
Montell, Craig

Publication Date

2016-07-01

DOI

10.1093/hmg/ddw132

Peer reviewed

OXFORD

Human Molecular Genetics, 2016, Vol. 25, No. 13 2752–2761

doi: 10.1093/hmg/ddw132
Advance Access Publication Date: 7 June 2016
Original Article

ORIGINAL ARTICLE

Suppression of the motor deficit in a mucolipidosis type IV mouse model by bone marrow transplantation

Marquis T. Walker[1,2,3] and Craig Montell[1,2,3,*]

[1]Neuroscience Research Institute, [2]Department of Molecular, Cellular, and Developmental Biology, University of California Santa Barbara, Santa Barbara, CA 93106, USA and [3]Department of Biological Chemistry, The Johns Hopkins University School of Medicine, Baltimore, MD 21205, USA

*To whom correspondence should be addressed at: Tel: +1 805 893 3634; Fax: 805 893-2005; Email: craig.montell@lifesci.ucsb.edu

Abstract

Mucolipidosis IV (MLIV) is a severe lysosomal storage disorder, which results from loss of the TRPML1 channel. MLIV causes multiple impairments in young children, including severe motor deficits. Currently, there is no effective treatment. Using a Drosophila MLIV model, we showed previously that introduction of *trpml*$^{+}$ in phagocytic glia rescued the locomotor deficit by removing early dying neurons, thereby preventing amplification of neuronal death from cytotoxicity. Because microglia, which are phagocytic cells in the mammalian brain, are bone marrow derived, and cross the blood–brain barrier, we used a mouse MLIV model to test the efficacy of bone marrow transplantation (BMT). We found that BMT suppressed the reduced myelination and the increased caspase-3 activity due to loss of TRPML1. Using a rotarod test, we demonstrated that early BMT greatly delayed the motor impairment in the mutant mice. These data offer the possibility that BMT might provide the first therapy for MLIV.

Introduction

Mucolipidosis type IV (MLIV) is an early-childhood-onset neurodegenerative disorder which results in profound neurological defects, including severe motor deficits (1). This lysosomal storage disorder (LSD) is caused by loss-of-function mutations in the *MCOLN1* gene, which encodes the late endosomal/lysosomal TRPML1 cation channel (2–4). TRPML1 functions in the efflux of Ca^{2+}, Na^{+} and some heavy metal cations from the lysosomal lumen to the cytosol, and helps to regulate lysosomal pH and ion homeostasis (5–8). Loss of TRPML1 expression in mice results in multiple deficits, including a progressive loss of hindlimb motor activity (9). The *Mcoln1*$^{-/-}$ animals display a measurable loss in strength in 2–3 months-old mutants, but the motor deficits are not clearly visible until 6.5 months of age (9).

We previously developed a Drosophila MLIV model, and showed that mutation of fly *trpml* also caused neurodegeneration and motor problems (6). Introduction of a *trpml*$^{+}$ transgene specifically in neurons fully rescued these impairments. As one of our negative controls, we expressed *trpml*$^{+}$ exclusively in glia. Unexpectedly, this also suppressed the rapid neurodegeneration and locomotor deficits. The glial-specific rescue results because phagocytic glia in the brain remove early dying neurons before they progress to late dying neurons and release cytotoxic agents that accelerates further neuronal death (6). On the basis of this finding, we proposed that restoring wild-type phagocytic glial activity in the mammalian brain would similarly suppress the rapid expansion of neurodegeneration (6). In further support of this concept, mammalian TRPML1 is also required in myelinating glia of the brain (10,11). Microglia are the professional phagocytes in the mammalian central nervous system and are derived from bone marrow stem cells. Therefore, we set out to restore phagocytic glial activity in the brain by introducing wild-type microglia through bone marrow transplantation (BMT) (6).

BMT has been investigated as part of an enzyme replacement regime in several LSD mouse models (12–17). However,

Received: January 16, 2016. **Revised:** April 4, 2016. **Accepted:** April 25, 2016

BMT had not been tested for MLIV, since unlike other LSDs, MLIV results from a mutation in the gene encoding the TRPML1 channel, rather than an enzyme. Here the concept for BMT was different—to replace impaired microglia needed for phagocytosis of dying neurons, rather than to supply a missing enzyme to the neurons. In this study, we demonstrate that BMT performed on young *Mcoln1*$^{-/-}$ mice suppresses defects in myelination, and accumulation of apoptotic neurons. Most strikingly, BMT greatly delays the onset of motor deficits, which we show are evident in the untreated mutants by 6 weeks of age. These findings support the proposal that BMT might represent a therapy to delay the motor deficits associated with MLIV.

Results

Early onset and progressive motor delay in *Mcoln1*$^{-/-}$ mice

To test the efficacy of BMT as a therapy for MLIV, we employed the rotarod performance test to establish a sensitive assay to measure the onset and progressive decline in motor activity. The rotarod apparatus is computer controlled and uses infrared sensors to monitor an animal's ability to remain on a rotating rod. This assay requires coordination to remain perched on the beam, and locomotor activity to keep up with the accelerating rotation of the rod. At the start of each test, we placed the mouse on the apparatus. The rod began rotating slowly at 5 RPMs, and accelerated 1 RPM every 5 s until the animal no longer stayed upright on the rod, and consequently fell off. Wild-type mice (C57Bl6; *Mcoln1*$^{+/+}$) remained on the rotarod for 130.2 ±11.3 s and 100.4 ±25.2 s at 15 an 32 weeks of age, respectively (Fig. 1A), and this ability was similar in heterozygous animals (*Mcoln1*$^{+/-}$; 114.8 ±9.7 s and 101.8 ±8.0 s, respectively; Fig. 1A).

To determine whether *Mcoln1*$^{-/-}$ mice were compromised in motor function, we compared their rotarod performance with control littermates (*Mcoln1*$^{+/-}$ heterozygous). We used mice that were ≥6 weeks old, since younger mice were too small to effectively negotiate the rotating rod.

We found that *Mcoln1*$^{-/-}$ mutant mice exhibited a deficit in rotarod performance, and underwent a progressive decline over the next 26 weeks. Even at the youngest age tested (6 weeks), the *Mcoln1*$^{-/-}$ mice were compromised, as their average runtimes were 23.3% shorter than the control littermates (74.3 ±6.3 s and 96.8 ±12.4 s, respectively; Fig. 1B). The mutant mice declined in performance with age. By 15 weeks, their average runtimes were only 54.2% as long as the controls (62.1 ±8.3 s and 114.5 ±9.7 s, respectively; Fig. 1B). Once they were 32 weeks old, all the *Mcoln1*$^{-/-}$ animals exhibited a dramatic deficit, and were able to remain on the rotarod for only 22.1% as long as control mice (22.5 ±4.9 s and 101.8 ±8.0 s, respectively; Fig. 1B). Due to the severe hindlimb paralysis, the animals were euthanized at 32 weeks.

Performing hematopoietic stem cell transplantation on the MLIV mouse model

We performed BMT treatments on control and *Mcoln1*$^{-/-}$ littermates at two ages: 8–10 days and 6 weeks. After conditioning the mice with the irradiation to deplete endogenous hematopoietic stem cells, we injected them with whole bone marrow from a congenic donor strain. To distinguish donor from recipient cells, we used donor bone marrow leukocytes that included an alloantigen leukocyte marker, CD45.1, which is an isoform of a tyrosine phosphatase distinct from the recipient CD45.2 isoform. Using isoform-specific antibodies along with flow cytometry, we established that the transplanted mice contained significant donor cells in the peripheral blood (Fig. 1C; 8–10 days old, 94.6 ±2.3%; 6 weeks old, 95.2 ±0.5%). The BMT-treated immature mice also had CD45.1 positive donor cells in their brains (Fig. 1D and E). These flow cytometry and immunohistochemistry results demonstrated that the donor hematopoietic stem cells were engrafted successfully.

Rescue of defects in motor neuron myelin thickness

Progressive hindlimb paralysis is a pronounced phenotypic indicator of neurodegeneration in the MLIV mouse model (9). These findings suggest that the effects on locomotor activity occur at least in part through impairments in the most distal regions of the nervous system. Neurological input into muscles of the hindlimb is transmitted through axons in the sciatic nerve. To analyze the effect that the loss of TRPML1 function has on peripheral nerves, we examined axons of the sciatic nerve, which are critical for normal hindlimb motor activity.

The sciatic nerve is composed of myelinated and non-myelinated axons. Myelin-expressing Schwann cells wrap around the outer surface of myelinated axons to form a thick outer layer. The thickness of the myelin layer is important to the conductance and signal transmission within these axons. Using electron microscopy, we measured the myelin thickness and calculated the *g*-ratio of myelinated axons. Control mice had an average g-ratio of 0.59 and only 1.6% of all axons had a *g*-ratio >0.7 (Fig. 2A–C). Consistent with previous reports (11,18), we found that *Mcoln1*$^{-/-}$ mice had a large increase in the percentage of thinly myelinated axons with a *g*-ratio >0.7 (12.6%) (Fig. 2D–F). Strikingly, BMT treatment fully reversed the accumulation of these thinly myelinated axons in *Mcoln1*$^{-/-}$ animals, as only 1.3% displayed a *g*-ratio >0.7 (Fig. 2G–I).

In addition to thinning myelin, the sciatic nerves of 15-week-old *Mcoln1*$^{-/-}$ mice displayed increased numbers of damaged axons in which the axons were separating from the myelin sheath and showed buckling and splitting of the myelin (Fig. 3A, B and D). Cerebellar neurons from 15-week-old mutant mice also exhibited dramatic reductions in the intensity of staining with NeuN—an antibody targeting a neuronal-specific RNA splicing factor, which decreases in intensity in degenerating neurons (Fig. 4) (19,20). However, there were no apparent reductions in axon numbers in the sciatic nerve (Fig. 3E) or DAPI-positive staining in the cerebellum (Fig. 4), indicating that the impaired neurons in *Mcoln1*$^{-/-}$ were similar in numbers to the controls. Of significance here, we found that the BMT treatment reduced the number of damaged axons in the sciatic nerve and restored NeuN staining in 15-week-old mutant animals that appeared typical of controls (Figs. 3C and D and 4).

Reduction in accumulation of apoptotic cells

To test whether the BMT reduced apoptotic cell accumulation, we stained sciatic nerve sections with antibodies against activated caspase-3, which marks apoptotic cells (21). In sections from control animals, we detected relatively little staining (Fig. 5A). In contrast, *Mcoln1*$^{-/-}$ tissue showed a dramatic increase in labeling (Fig. 5B and D). Of significance here, BMT treatment greatly decreased the accumulation of anti-activated caspase-3 staining (Fig. 5C and D).

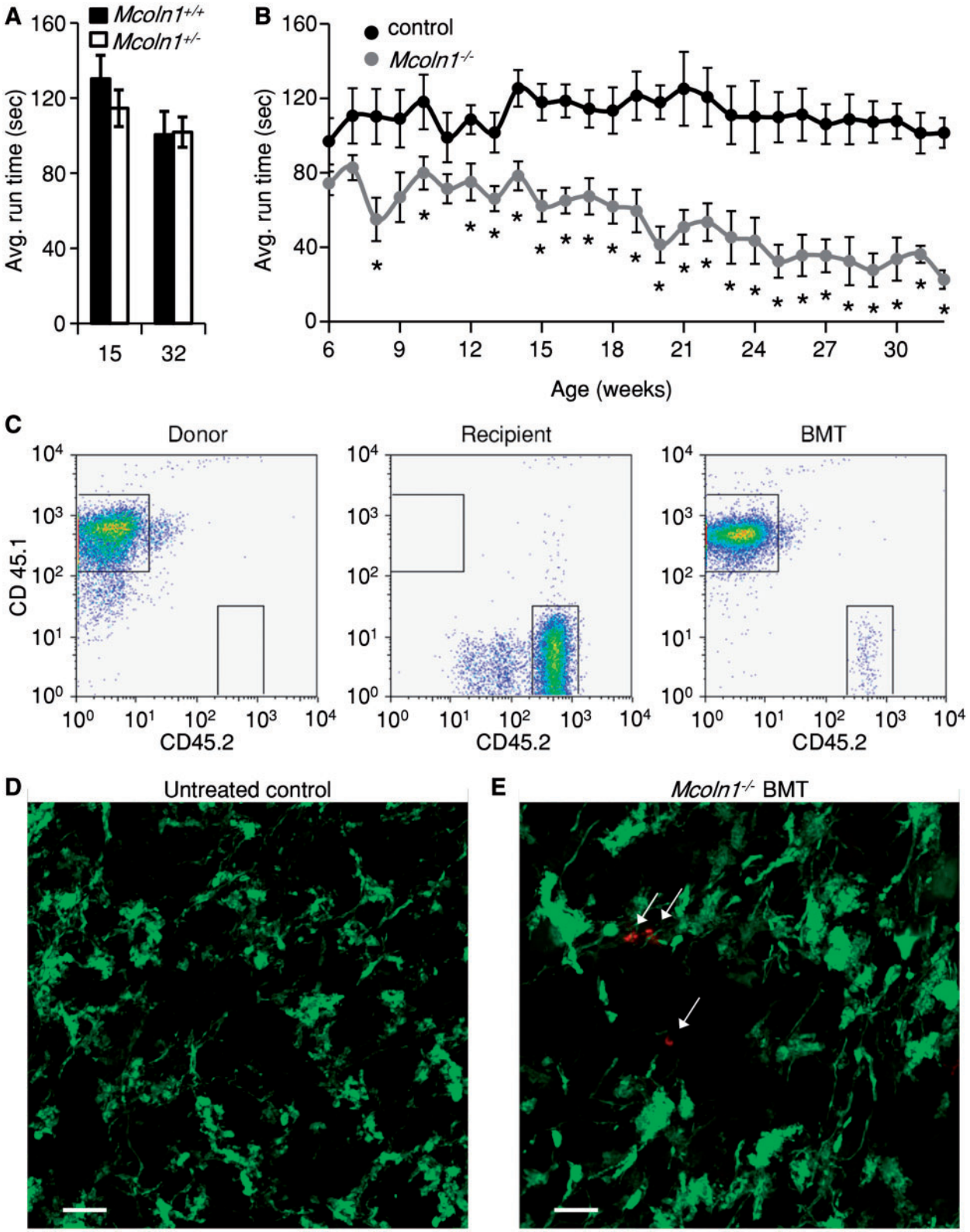

Figure 1. Rotarod locomotor activity assays and BMT efficacy. (**A**) Rotarod assay activities for *Mcoln1*$^{+/+}$ (black bars) and *Mcoln1*$^{+/-}$ (white bars) animals at 15 and 32 weeks of age. (**B**) Weekly rotarod assays comparing control and mutant animals. Control (*Mcoln1*$^{+/-}$, black) and *Mcoln1*$^{-/-}$ (grey). We used the unpaired Student t-tests with two-tail analysis. The error bars indicate S.E.M.s and the asterisks indicate $P < 0.05$. (**C**) Two-color flow cytometry analyses of peripheral blood monocytes from mice at 12–15 weeks of age. Donor, LY5.2 mouse; Recipient, untreated *Mcoln1*$^{-/-}$ mice; BMT, bone marrow transplanted recipient mouse. (**D**) Cross-section of a cerebellum from an untreated *Mcoln1*$^{-/-}$ mouse expressing a Thy1-YFP transgene. (**E**) *Mcoln*$^{-/-}$ mouse at 15 weeks of age expressing a Thy1-YFP transgene transplanted at 8–10 days old with bone marrow from LY5.2 mice congenic mice expressing CD45.1. Thy1-YFP (green) labels neurons and processes. The arrows indicate anti-CD45.1 positive donor cells (red). The scale bars in (D) and E represent 10 μm.

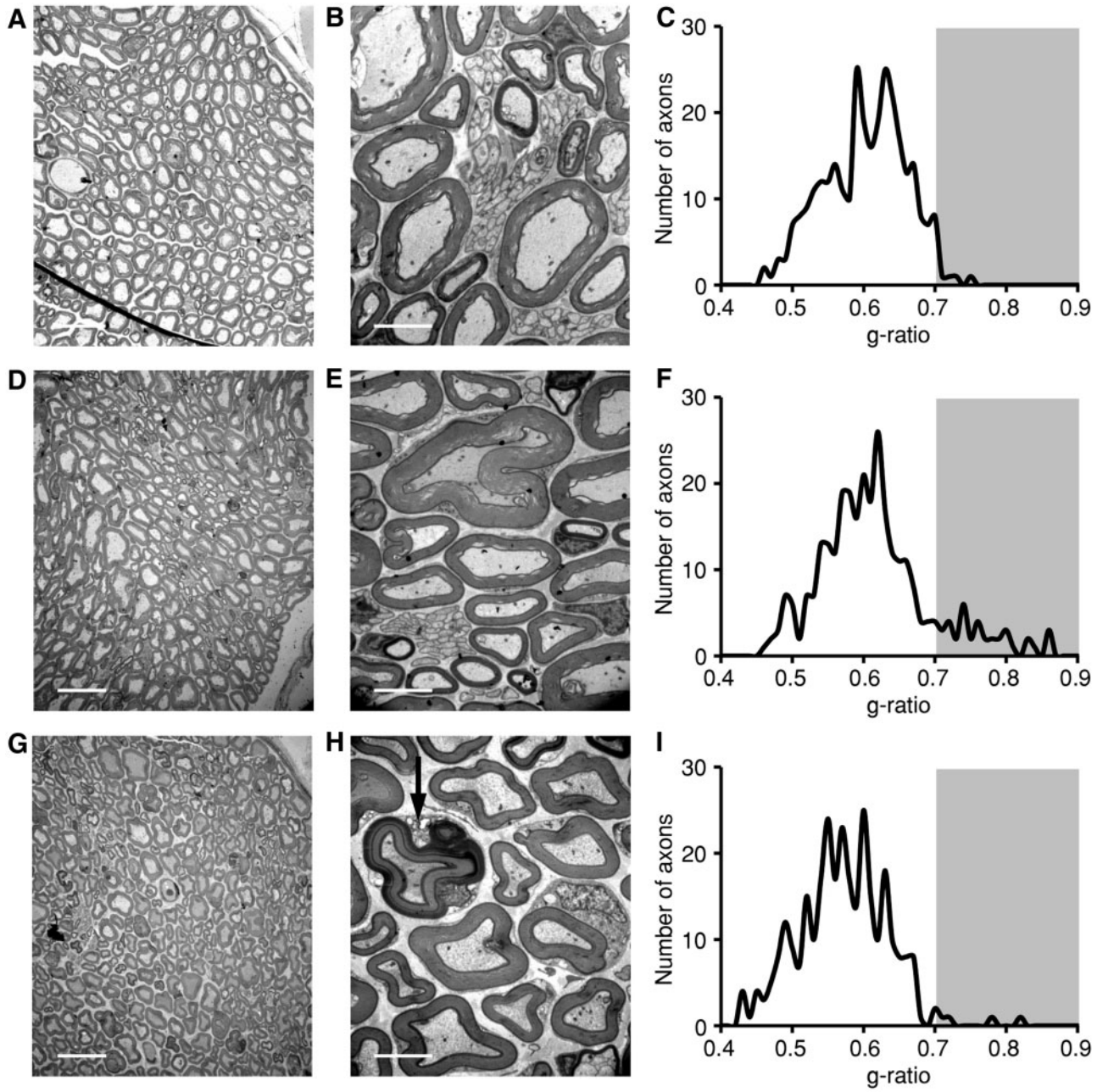

Figure 2. Myelinated axons in the sciatic nerve. (**A and B**) Electron micrographs of osmium stained sciatic nerve axons from 15-week-old controls (*Mcoln1*$^{+/-}$). (**C**) Plot of axon myelin *g*-ratios (√inner area/total area) from control sciatic nerves. The shaded area highlights g-ratios above 0.7. (**D and E**) Electron micrographs of osmium stained sciatic nerve axons from 15-week-old *Mcoln1*$^{-/-}$. (**F**) Plot of axon myelin *g*-ratios from *Mcoln1*$^{-/-}$ sciatic nerves. The shaded area highlights *g*-ratios above 0.7. (**G** and **H**) Electron micrographs of osmium stained sciatic nerve axons from a 15-week-old *Mcoln1*$^{-/-}$ mouse that underwent BMT at 8–10 days of age. The red arrow indicates a myelinated axon being engulfed by phagocytosis. (**I**) Plot of axon myelin g-ratio over the axon diameter from sciatic nerves of *Mcoln1*$^{-/-}$ mice that underwent BMT at 8–10 days of age. The shaded area highlights g-ratios above 0.7. The scale bars in A, D, G and B, E, H indicate 20 μm and 4 μm, respectively.

During cell clearance, phagocytic macrophage/microglia are activated and infiltrate tissue to move toward and engulf apoptotic cells. We used anti-Iba1 staining to detect macrophage/microglia activity in the sciatic nerve. Consistent with the increased caspase-3 activity, *Mcoln1*$^{-/-}$ mice exhibited elevated macrophage/microglia activity (Fig. 5E, F and H). We found that the BMT treated mice also had elevated anti-Iba1 staining (Fig. 5G and H). Because the treated mice were *Mcoln1*$^{-/-}$ mutants, there was still an increase in primary neuronal cell death. As a consequence, the macrophages/microglia were active in order to remove the dying cells.

Delay in motor deficits in *Mcoln1*$^{-/-}$ mice by BMT

A key question was whether BMT would suppress the decline in motor function. If successful, the treatment would delay the loss in motor function since the decrease in function due to the bystander effect would be reduced or eliminated. However, this treatment would not necessarily permanently rescue the impairment since the primary cell death would still take place. To assess the efficacy of the BMT, we used the rotarod, and tested animals at 6, 15 and 32 weeks of age. As described above, untreated control animals displayed constant run times over

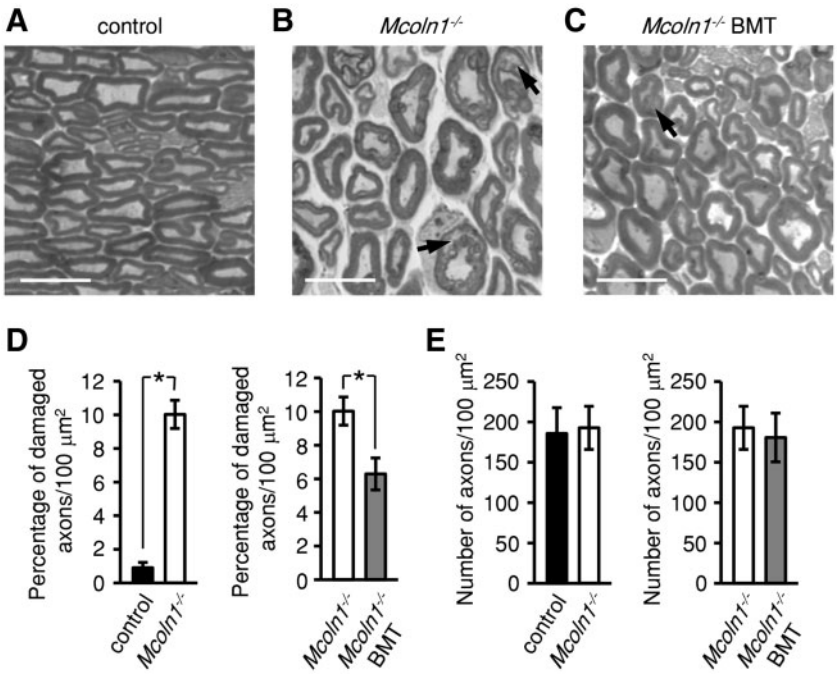

Figure 3. Myelinated axons in the sciatic nerve. (**A–C**) Light micrographs of methylene blue stained sciatic nerve axons from a 15-week-old control (*Mcoln1*$^{+/-}$), *Mcoln1*$^{-/-}$ and *Mcoln1*$^{-/-}$ that underwent BMT at 8–10 days of age. The arrows indicate buckling and splitting of myelin in damaged axons where the axons are separating from the surrounding myelin sheath. (**D**) Percentage of damaged axons per 100 μm^2. (**E**) Total number of axons per 100 μm^2. The scale bars in A, B, and C indicate 10 μm. Statistical analyses were performed using unpaired Student's *t*-tests with two-tail analysis. The asterisks indicate statistically significant differences ($P < 0.05$).

this 26 week period, while untreated *Mcoln1*$^{-/-}$ mice underwent a decline (Fig. 6A). When we performed the BMT on 6-week-old mutant mice, there was no improvement (Fig. 6B).

Remarkably, we found that application of BMT treatment to 8-10 day old *Mcoln1*$^{-/-}$ animals resulted in a profound benefit. 6 and 15-week-old *Mcoln1*$^{-/-}$ animals performed similar to untreated control mice, or to control animals that underwent BMT (Fig. 6C and D). Even at 32 weeks of age, the treated *Mcoln1*$^{-/-}$ mice exhibited run times indistinguishable from treated controls (Fig. 6C and D). However, at 32 weeks of age, the control mice that were exposed to the BMT failed to maintain the same rotarod performance as the untreated control animals. We reduced the irradiation from 3 Gy to 1 Gy and this change eliminated the adverse effect to 32-week-old controls, but did not further improve the performance of the treated 32-week-old *Mcoln1*$^{-/-}$ mice (Fig. 6E and F).

Discussion

Currently, there is no effective treatment for MLIV. To develop a therapeutic concept for this devastating disorder, we took advantage of the finding that the neurodegeneration and motor problems in a fly MLIV model were reduced by expressing the wild-type TRPML1 homolog specifically in glia (6). In flies, the suppression resulted from removal of early apoptotic neurons before they progressed to late apoptotic neurons and released cytotoxic agents that accelerated cell death due to a bystander effect (6). Because microglia are phagocytic and bone marrow derived, we used the mouse MLIV model (9) to test the effectiveness of BMT.

The first challenge to testing the idea that BMT might provide a treatment was to ascertain whether TRPML1-deficient mice displayed early onset motor problems, as is the case in MLIV patients. *Mcoln1*$^{-/-}$ mice exhibit changes in gait (9). However, this phenotype is not clearly detectable until ~6.5 months of age. We found that the rotarod provided a sensitive assay, which revealed deficits in motor function in 6-week-old *Mcoln1*$^{-/-}$ mice. The sensitivity of this assay allowed us to distinguish and quantify motor deficits in mutant animals much earlier than before, and the impairments are consistent with the early onset motor defects in MLIV patients (22).

We found that BMT greatly delayed the onset of the motor problems, but only if the BMT was performed on young, 8–10-d-old mutant animals. When the BMT was performed at 6 weeks of age, there was no amelioration of rotarod performance. This suggests that if BMT were to be performed on MLIV patients, it would need to be conducted on young patients. This may be feasible, since most MLIV patients are diagnosed very early at 1–2 years of age, when the individuals begin to show early deficits in achieving developmental milestones (1).

The BMT appeared to fully suppress the motor deficits of 6- and 15-week-old *Mcoln1*$^{-/-}$ animals. However, by 32 weeks, the treated mutants were no longer performing on the rotarods as well as control animals. Nevertheless, the 32-week-old treated *Mcoln1*$^{-/-}$ mice displayed run times similar to the untreated mutant at 6 weeks of age. The eventual reduction in performance in older animals was not surprising, since the primary deficit in neurons remained. We suggest that the BMT suppressed the motor impairment due to removal of early apoptotic neurons by microglia, thereby diminishing a bystander effect. Consistent with this conclusion, we found that BMT decreased the accumulation of apoptotic neurons, as indicated by caspase-3 staining. We also suggest that BMT restored phagocytosis of myelin by the macrophages/microglia. Myelin removal is an important aspect of nerve repair in the peripheral nervous system, as it is critical for new axons to reinnervate nerves (23). While the improvement in motor function was dramatic, not every aspect of the *Mcoln1*$^{-/-}$ phenotype was ameliorated, as we did not detect

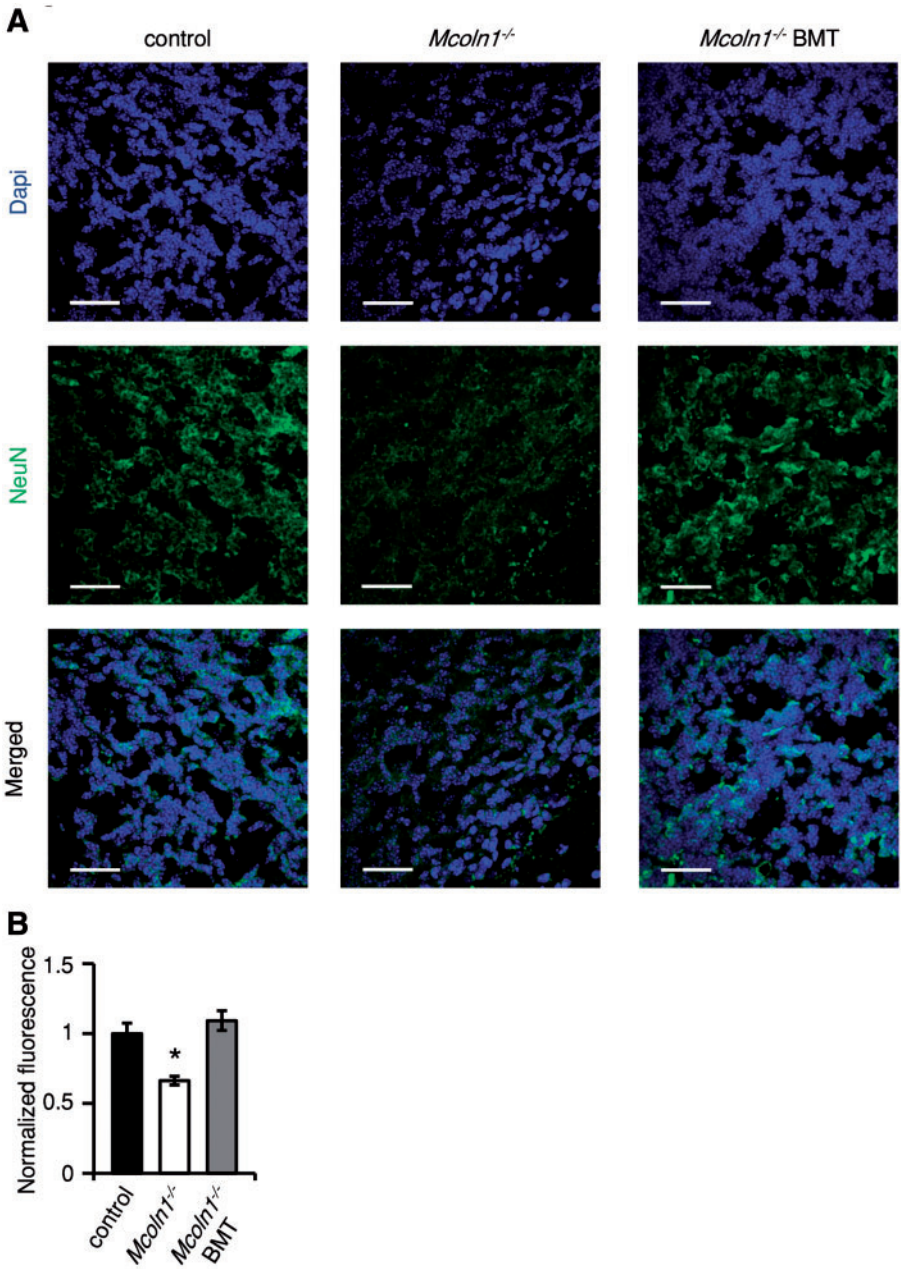

Figure 4. Reduced NeuN staining in 15-week-old *Mcoln1*$^{-/-}$ cerebellum suppressed by BMT. **(A)** Cerebellar sections from 15-week-old controls (*Mcoln1*$^{+/-}$), *Mcoln1*$^{-/-}$ and *Mcoln1*$^{-/-}$ that underwent BMT at 8–10 days of age were stained with anti-NeuN (neuronal nuclei) and DAPI (nuclear stain). The scale bars in each image indicate 30 μm. **(B)** Relative fluorescence intensities of the anti-NeuN staining. Statistical analyses were performed using a one-way ANOVA test with the Bonferroni–Holm *post hoc* test. The error bars indicate SEMs and the asterisks indicate statistically significant differences ($P < 0.05$).

reduced retinal degeneration, as indicated by the thinner outer nuclear layer (Supplementary Material, Fig. S1).

In conclusion, this study provides the first potential therapeutic approach to delay the motor deficits in MLIV patients, and also the first possible therapy for a "TRPopathy." An additional step will be to identify strategies to reduce the primary cell death of the neurons. Along these lines is a recent study in which small molecules ameliorate the effects of defective TRPML1 in a cell line isolated from patients (24). Loss of Drosophila TRPML and mammalian TRPML1 function reduces TORC1 activity and causes incomplete autophagy (6,25–31), effects that are reduced in flies by amino acid supplementation (26). Thus, a combination of BMT along with a protein-rich diet and small molecule therapy could potentially provide even greater suppression of the MLIV deficits.

Materials and Methods

Mouse lines and genotyping

The *Mcoln*$^{-/-}$ mouse line were generated previously (9). To distinguish the *Mcoln1*$^{+/+}$ (wild-type), *Mcoln1*$^{+/-}$ (heterozygote, control) and *Mcoln1*$^{-/-}$ offspring, we used a three-primer PCR mixture with genomic DNA extracted from tail clippings (primers: forward, 5′-TGAGGAGAGCCAAGCTCATT-3′; reverse 1 neo, 5′-TGGCTGGACGTAAACTCCTC-3′; and reverse

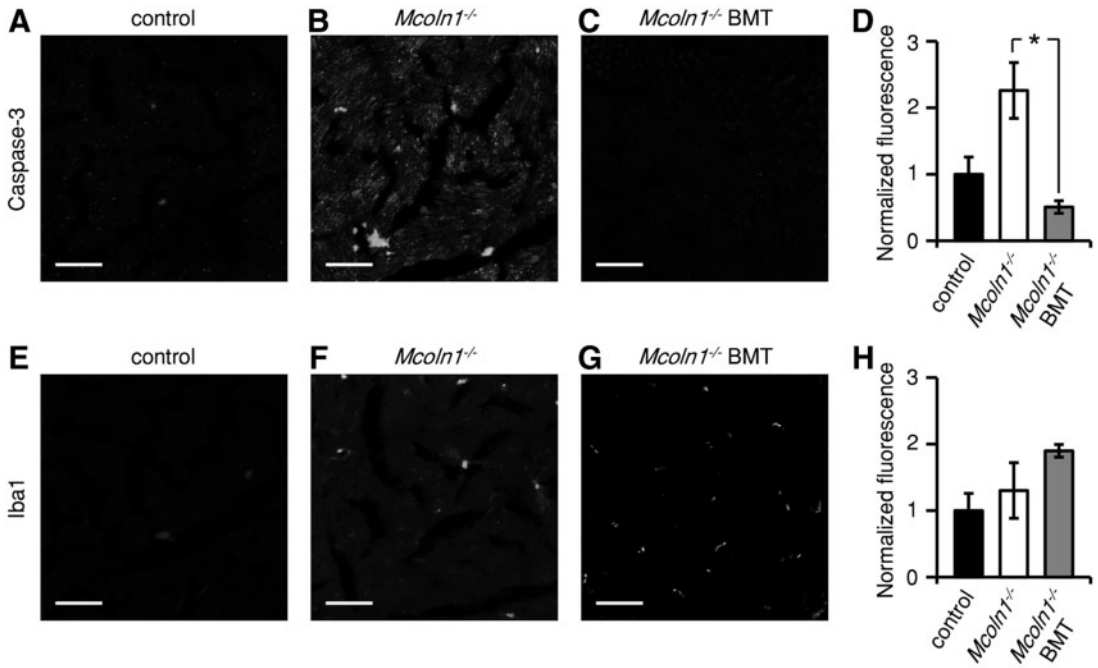

Figure 5. Staining of sections of sciatic nerve with anti-caspase-3 and anti-Iba1. The sections were isolated from 15-week-old animals. The $Mcoln^{-/-}$ BMT mice underwent BMT at 8–10 days of age. (**A–C**) Anti-caspase-3 staining of sciatic nerves from control ($Mcoln1^{+/-}$), $Mcoln1^{-/-}$ and a BMT treated $Mcoln^{-/-}$ mouse. (**D**) Plot of relative fluorescence intensity of the anti-caspase-3 staining. (**E–G**) Staining of phagocytic microglia in the sciatic nerve with anti-Iba1. (**H**) Plot of relative fluorescence intensity of Iba1 staining. The scale bars in **A–C** and **E–G** indicate 50 μm. Statistical analyses were performed using a one-way ANOVA test with the Bonferroni–Holm *post hoc* test. The error bars indicate S.E.M.s and the asterisks indicate statistically significant differences ($P < 0.05$).

2 intron 3, 5′-TCATCTTCCTGCCTCCATCT-3′). The B6.Cg-Tg(Thy1-YFP)16Jrs/J mouse line was purchased from Jackson Labs and crossed into the $Mcoln1^{-/-}$ line. Mice expressing the transgene were used to visualize motor neuron axons and were identified by PCR genotyping (primers: Thy1F1, 5′-TCTGAGTGG CAAAGGACCTTAGG-3′; and EYFPR1, 5′-CGCTGAACTTGTGGCCG TTTACG-3′). To isolate DNA, we obtained tail clippings, lysed them in 200 µl of DirectPCR (Viagen) plus 6 µl of 20 mg/ml proteinase K (Roche) and incubated the samples overnight at 55 °C. We then heated the samples at 85 °C for 45 min to heat kill the proteinase K activity, and then placed them on ice. The lysates were later used as the sources of the DNA templates for the PCR reactions. PCR was performed using Taq DNA polymerase (Apex). B6-Ly5.2/Cr (NCI-Frederick) mice were used as bone marrow donor animals. All breeding and other mouse procedures were approved by the Johns Hopkins University School of Medicine Animal Care and Use Committee.

Chemicals

DirectPCR (Viagen), proteinase K (Roche), RBC Lysis Buffer (Affymetrix eBioscience), VECTASHIELD mounting medium (Vector Laboratories) and Hoechst 33342 (Thermo Fisher) were obtained from the indicated sources. We purchased phosphate-buffered saline and fetal bovine serum from Invitrogen. The following chemicals were purchased from Sigma-Aldrich: sucrose, normal goat serum, Triton X-100, sucrose, Permount and ethanol. The following chemicals were purchased from Electron Microscopy Sciences: paraformaldehyde, OCT freezing medium, sodium cacodylate, osmium tetroxide, glutaraldehyde, potassium ferrocyanide, propylene oxide, methylene blue, ERL 4206, DER 736, NSA and DMAE.

Rotarod performance test

We performed rotarod testing using a Rotamex 5 (Columbus Instruments, OH). The rotating rod was suspended ~35 cm above the base of the apparatus. The rotation speed, which was monitored by a computer, started at 5 RPMs and increased 1 RPM every 5 s. Once the mouse fell off of the rod, the test was terminated and the run time was recorded. Weekly testing of the animals was initiated when the animals reached 6 weeks of age, and terminated at 32 weeks of age.

Hematopoietic stem cell transplantation

We administered BMT either when the mice were 8–10 days old or 6 weeks old. To deplete endogenous hematopoietic stem cells, we irradiated the animals with a ^{137}Cs source at the following doses: 8–10 days old, 1 or 3 Gy; 6 weeks old, 9.7 Gy. Donor bone marrow cells were harvested from the femurs and tibias of 6-10-week old C57BL/6-Ly5.2/Cr (NCI-Frederick) congenic mice. The cells were resuspended in phosphate-buffered saline (PBS) with 2.5% fetal bovine serum (FBS) and filtered through a 70 µm cell strainer. Recipient mice were injected with donor bone marrow cells 4–8 h post-irradiation. Six-week-old mice were injected in the tail vein with 1×10^6 cells (in 250 µl) and 8 -10-day old mice were injected with 1×10^6 cells in 250 µl in the retro-orbital sinus.

Examining bone marrow engraftment

To examine the extent of donor bone marrow engraftment in transplanted mice, we collected ~100 µl blood using a 5 mm lancet to puncture the submandibular vein. To remove red blood cells (RBCs), we added 900 µl RBC Lysis Buffer and transferred

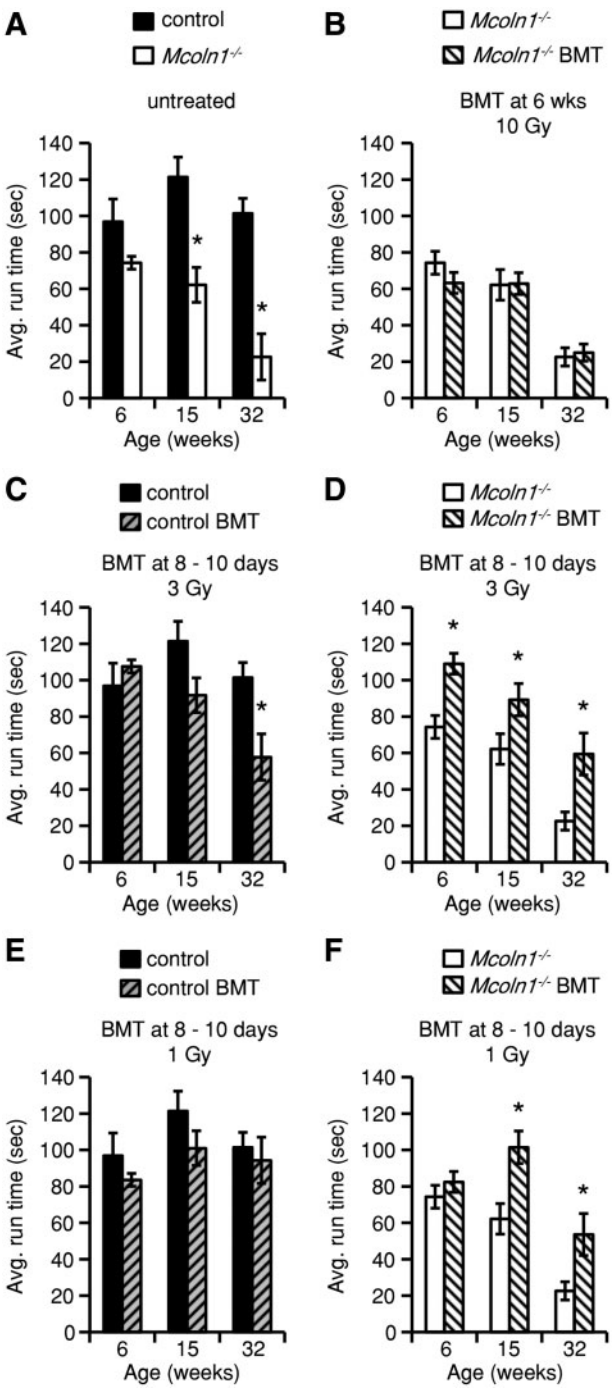

Figure 6. Effects of BMT on performance using rotarod locomotor activity assays. Shown are the average run times of the indicated animals. (**A**) Untreated control (*Mcoln1*$^{+/-}$) and *Mcoln1*$^{-/-}$. (**B**) Untreated *Mcoln1*$^{-/-}$ and *Mcoln1*$^{-/-}$mice that underwent BMT at 6 weeks of age. (**C**) Untreated control (*Mcoln1*$^{+/-}$) and control that were conditioned with 3 Gy irradiation and underwent BMT at 8–10 days of age. (**D**) Untreated *Mcoln1*$^{-/-}$ and *Mcoln1*$^{-/-}$ that were conditioned with 3 Gy irradiation and underwent BMT at 8–10 days of age. (**E** and **F**) The same as (**C**) and (**D**) except that the mice were conditioned with 1 Gy irradiation. Statistical analysis was performed using an unpaired Student's *t*-test with two-tail analysis. The asterisks indicate statistically significant differences ($P < 0.05$).

the mixture to a 1.5 ml microfuge tube. The mixture was incubated at room temperature for 5 min and centrifuged at 400 × *g* for 1 min. The supernatant was removed and the remaining hematopoietic stem cells were resuspended in 100 µl of PBS containing 2.5% FBS. The cells were labeled by adding 100 µl staining solution (1:2000 dilution of anti-CD45.2-FITC and anti-CD45.1-PE in PBS with 2.5% FBS). The samples were incubated at room temperature for 20 min and centrifuged at 400 × *g* for 1 min. The supernatants were removed and the cell pellets were resuspended in 1 ml of PBS plus 2.5% FBS. We then distinguished CD45.2-FITC and CD45.1-PE labeled cells by flow cytometry (BD FACScaliber) of the peripheral blood mononuclear cells.

Immunohistochemical staining of brains for donor-derived cells

Mice were euthanized and transcardially perfused with PBS followed by 4% paraformaldehyde (PFA) in PBS. Brains were dissected from the skull and incubated in PFA overnight at 4 °C, followed by three washes with PBS. The brains were incubated overnight in 30% sucrose in PBS, and embedded in OCT freezing medium. We prepared 20 µm sections, which we blocked and permeabilized with blocking buffer (5% normal goat serum and 0.3% Triton X-100 in PBS) for 1 h at room temperature. We incubated the sections with anti-CD45.1 antibody (eBiosciences) in blocking buffer overnight at 4 °C. Sections were washed 5× with PBS and incubated for 1 h at room temperature with Alexafluor 568 anti-rat antibodies (Invitrogen) at a 1:1000 dilution in blocking buffer. The slides were washed 5× with PBS and mounted in VECTASHIELD mounting medium. Brains were imaged using a Zeiss LSM 700 confocal microscope at 40× magnification.

Electron microscopic analysis of myelination thickness in sciatic nerves

To assess the thickness of the myelin layer in the sciatic nerve, we transcardially perfused mice with PBS followed by 4% PFA in PBS. We dissected the sciatic nerve, fixed the tissue in 2% PFA containing 2% glutaraldehyde plus 2.5% sucrose in 0.1 M sodium cacodylate pH 7.4 for 2 h, and washed the tissue three times in 0.1 M sodium cacodylate, 2.5% sucrose and 5 mM $CaCl_2$. The tissue was stained in freshly made reduced osmium tetroxide (OsO_4) staining solution. The staining solution was made in two parts: (a) 80 mg of potassium ferrocyanide in 4 ml of 0.1 M sodium cacodylate pH 7.4 and 2.5% sucrose, and (b) 2 ml of 4% OsO_4 in 2 ml of 0.2 M sodium cacodylate pH 7.4 plus 2.5% sucrose. The tissue was resuspended in OsO_4 staining solution and incubated on ice for 2 h in the dark. We then washed the tissue three times for 10 min with H_2O and incubated the samples in 2% uranyl acetate for 30 min. We dehydrated the tissue with a series of 5 min washes in increasing concentrations of ethanol: 50%, 70% and 90%. We then washed the tissue three times for 5 min each with 100% ethanol and twice with propylene oxide for 5 min. The tissue was resuspended in a 1:1 mixture of propylene oxide and low viscosity Spurr's embedding resin (5 ml ERL 4206, 3 ml DER 736, 13 ml NSA and 0.2 ml DMAE) for 1 h at room temperature. The mixture was replaced with 100% Spurr's embedding resin and incubated overnight at room temperature. Tissues were transferred to fresh 100% Spurr's embedding resin and set in a mold for polymerization. The samples were incubated at 60 °C overnight to cure the resin. Sections of 50–70 nm were collected and imaged on a Phillips 120 transmission electron microscope. Images were analyzed using ImageJ software and the GRatio plugin (http://gratio.efil.de/) to calculate the myelin g-ratio and axon diameter.

Light microscopic analysis of damaged axons in the sciatic nerve

We used sciatic nerves that were stained and embedded in Spurr's resin as described above. Cross-sections of 0.5 μm were dried onto a glass slide. The samples were stained with 1% methylene blue for 30 s, rinsed thoroughly with H_20, and allowed to dry completely. We mounted a coverslip using Permount mounting media, allowed the mounting media to cure at room temperature overnight and captured images at 160× magnification with a light microscope (Zeiss Axiovert). Captured images were analyzed using image J to count the total number of normal and damaged myelinated axons within 100 μm^2 areas. We identified damaged axons by looking for buckling and splitting in the myelin, and axon separation from the myelin sheath.

Immunohistochemical staining of sciatic nerves and the cerebellum

Mice were euthanized and transcardially perfused with PBS followed by 4% paraformaldehyde in PBS. After the dissections, the tissues were incubated in paraformaldehyde overnight at 4 °C, washed three times with PBS, incubated overnight in 30% sucrose in PBS, and embedded in OCT freezing medium. We prepared 20 μm sections, which we blocked and permeabilized with blocking buffer (5% normal goat serum and 0.3% Triton X-100 in PBS) for 1 h at RT. We incubated the sections of sciatic nerves with the following primary antibodies in blocking buffer overnight at 4 °C: rabbit anti-caspase-3, 1:200 dilution (Cell Signaling) or rabbit anti-Iba1, 1:100 dilution (Wako). The sections were washed five times with PBS and incubated for 1 h at RT with secondary antibodies (Alexafluor 647 anti-rabbit, 1:1000 dilution, Invitrogen) in blocking buffer. The slides were washed five times with PBS and mounted in VECTASHIELD mounting medium. For mouse cerebellar sections we incubated the samples overnight at 4 °C with primary antibodies (mouse anti-NeuN, 1:1000 dilution, Millipore) in blocking buffer. The sections were washed five times with PBS and incubated for 1 h at RT with secondary antibodies (Alexafluor 633 anti-mouse, 1:1000 dilution, Invitrogen) in blocking buffer. The slides were washed five times with PBS and mounted in VECTASHIELD mounting medium.

Images were captured on a Zeiss LSM 780 confocal microscope. We measured fluorescence with the Image J software. Relative fluorescence = (fluorescence of the antibody stained sciatic nerve cross section) − (the image average background fluorescence of the sciatic nerve). The average background was determined by sampling the background at three positions in the image, calculating the average and multiplying the average by the area of the sciatic nerve.

Statistical analyses

We used unpaired Student *t*-tests with two-tail analyses for the rotarod and sciatic nerves. To analyze the anti-caspase-3 or anti-Iba1staining of sciatic nerves and NeuN staining of cerebellar neurons, we used a one-way ANOVA test with the Bonferroni-Holm *post hoc* test. Error bars indicate S.E.M.s and the asterisks indicate statistically significant differences ($P < 0.05$).

Supplementary Material

Supplementary Material is available at *HMG* online.

Acknowledgements

The authors thank S. A. Slaugenhaupt (Massachusetts General Hospital and Harvard Medical School) for generously providing the *Mcoln*$^{-/-}$ mice, and R. Li for technical help with early phases of this study.

Conflict of Interest Statement. None declared.

Funding

M.T.W. from supported in part by a postdoctoral fellowship from the National Institute of Neurological Disorders and Stroke (1F32 NS067903-01A1). This work was supported by grants to C.M. from the March of Dimes and the National Eye Institute (grant numbers EY008117, EY010852).

References

1. Bach, G., Zeevi, D.A., Frumkin, A. and Kogot-Levin, A. (2010) Mucolipidosis type IV and the mucolipins. *Biochem. Soc. Trans.*, **38**, 1432–1435.
2. Bargal, R., Avidan, N., Ben-Asher, E., Olender, Z., Zeigler, M., Frumkin, A., Raas-Rothschild, A., Glusman, G., Lancet, D. and Bach, G. (2000) Identification of the gene causing mucolipidosis type IV. *Nat. Genet.*, **26**, 118–123.
3. Bassi, M.T., Manzoni, M., Monti, E., Pizzo, M.T., Ballabio, A. and Borsani, G. (2000) Cloning of the gene encoding a novel integral membrane protein, mucolipidin-and identification of the two major founder mutations causing mucolipidosis type IV. *Am. J. Hum. Genet.*, **67**, 1110–1120.
4. Sun, M., Goldin, E., Stahl, S., Falardeau, J.L., Kennedy, J.C., Acierno, J.S., Jr, Bove, C., Kaneski, C.R., Nagle, J., Bromley, M.C. *et al.* (2000) Mucolipidosis type IV is caused by mutations in a gene encoding a novel transient receptor potential channel. *Hum. Mol. Genet.*, **9**, 2471–2478.
5. Kiselyov, K., Colletti, G.A., Terwilliger, A., Ketchum, K., Lyons, C.W., Quinn, J. and Muallem, S. (2011) TRPML: transporters of metals in lysosomes essential for cell survival? *Cell Calcium*, **50**, 288–294.
6. Venkatachalam, K., Long, A., Elsaesser, R., Nikolaeva, D., Broadie, K. and Montell, C. (2008) Motor deficit in a *Drosophila* model of mucolipidosis type IV due to defective clearance of apoptotic cells. *Cell*, **135**, 838–851.
7. Venkatachalam, K., Wong, C.O. and Zhu, M.X. (2015) The role of TRPMLs in endolysosomal trafficking and function. *Cell Calcium*, **58**, 48–56.
8. Wang, W., Zhang, X., Gao, Q. and Xu, H. (2014) TRPML1: an ion channel in the lysosome. *Handb. Exp. Pharmacol.*, **222**, 631–645.
9. Venugopal, B., Browning, M.F., Curcio-Morelli, C., Varro, A., Michaud, N., Nanthakumar, N., Walkley, S.U., Pickel, J. and Slaugenhaupt, S.A. (2007) Neurologic, gastric, and opthalmologic pathologies in a murine model of mucolipidosis type IV. *Am. J. Hum. Genet.*, **81**, 1070–1083.
10. Grishchuk, Y., Pena, K.A., Coblentz, J., King, V.E., Humphrey, D.M., Wang, S.L., Kiselyov, K.I. and Slaugenhaupt, S.A. (2015) Impaired myelination and reduced ferric iron in mucolipidosis IV brain. *Dis. Model. Mech.*, **8**, 1591–1601.
11. Grishchuk, Y., Sri, S., Rudinskiy, N., Ma, W., Stember, K.G., Cottle, M.W., Sapp, E., Difiglia, M., Muzikansky, A., Betensky, R.A *et al.* (2014) Behavioral deficits, early gliosis, dysmyelination and synaptic dysfunction in a mouse model of mucolipidosis IV. *Acta Neuropathol. Commun.*, **2**, 133.

12. Vogler, C., Sands, M.S., Galvin, N., Levy, B., Thorpe, C., Barker, J. and Sly, W.S. (1998) Murine mucopolysaccharidosis type VII: the impact of therapies on the clinical course and pathology in a murine model of lysosomal storage disease. *J. Inherit. Metab. Dis.*, **21**, 575–586.
13. Wada, R., Tifft, C.J. and Proia, R.L. (2000) Microglial activation precedes acute neurodegeneration in Sandhoff disease and is suppressed by bone marrow transplantation. *Proc. Natl. Acad. Sci. U. S. A.*, **97**, 10954–10959.
14. Walkley, S.U., Thrall, M.A., Dobrenis, K., Huang, M., March, P.A., Siegel, D.A. and Wurzelmann, S. (1994) Bone marrow transplantation corrects the enzyme defect in neurons of the central nervous system in a lysosomal storage disease. *Proc. Natl. Acad. Sci. U. S. A.*, **91**, 2970–2974.
15. Sands, M.S., Erway, L.C., Vogler, C., Sly, W.S. and Birkenmeier, E.H. (1995) Syngeneic bone marrow transplantation reduces the hearing loss associated with murine mucopolysaccharidosis type VII. *Blood*, **86**, 2033–2040.
16. Norflus, F., Tifft, C.J., McDonald, M.P., Goldstein, G., Crawley, J.N., Hoffmann, A., Sandhoff, K., Suzuki, K. and Proia, R.L. (1998) Bone marrow transplantation prolongs life span and ameliorates neurologic manifestations in Sandhoff disease mice. *J. Clin. Invest.*, **101**, 1881–1888.
17. Ohlemiller, K.K., Vogler, C.A., Roberts, M., Galvin, N. and Sands, M.S. (2000) Retinal function is improved in a murine model of a lysosomal storage disease following bone marrow transplantation. *Exp. Eye Res.*, **71**, 469–481.
18. Micsenyi, M.C., Dobrenis, K., Stephney, G., Pickel, J., Vanier, M.T., Slaugenhaupt, S.A. and Walkley, S.U. (2009) Neuropathology of the *Mcoln1*$^{-/-}$ knockout mouse model of mucolipidosis type IV. *J. Neuropathol. Exp. Neurol.*, **68**, 125–135.
19. Mullen, R.J., Buck, C.R. and Smith, A.M. (1992) NeuN, a neuronal specific nuclear protein in vertebrates. *Development*, **116**, 201–211.
20. Maximova, O.A., Murphy, B.R. and Pletnev, A.G. (2010) High-throughput automated image analysis of neuroinflammation and neurodegeneration enables quantitative assessment of virus neurovirulence. *Vaccine*, **28**, 8315–8326.
21. Wang, J., Silva, J.P., Gustafsson, C.M., Rustin, P. and Larsson, N.G. (2001) Increased *in vivo* apoptosis in cells lacking mitochondrial DNA gene expression. *Proc. Natl. Acad. Sci. U. S. A.*, **98**, 4038–4043.
22. Wakabayashi, K., Gustafson, A.M., Sidransky, E. and Goldin, E. (2011) Mucolipidosis type IV: an update. *Mol. Genet. Metab.*, **104**, 206–213.
23. Vargas, M.E., Watanabe, J., Singh, S.J., Robinson, W.H. and Barres, B.A. (2010) Endogenous antibodies promote rapid myelin clearance and effective axon regeneration after nerve injury. *Proc. Natl. Acad. Sci. U. S. A.*, **107**, 11993–11998.
24. Chen, C.C., Keller, M., Hess, M., Schiffmann, R., Urban, N., Wolfgardt, A., Schaefer, M., Bracher, F., Biel, M., Wahl-Schott, C. *et al.* (2014) A small molecule restores function to TRPML1 mutant isoforms responsible for mucolipidosis type IV. *Nat. Commun.*, **5**, 4681.
25. Vergarajauregui, S., Connelly, P.S., Daniels, M.P. and Puertollano, R. (2008) Autophagic dysfunction in mucolipidosis type IV patients. *Hum. Mol. Genet.*, **17**, 2723–2737.
26. Wong, C.O., Li, R., Montell, C. and Venkatachalam, K. (2012) *Drosophila* TRPML is required for TORC1 activation. *Curr. Biol.*, **22**, 1616–1621.
27. Venugopal, B., Mesires, N.T., Kennedy, J.C., Curcio-Morelli, C., Laplante, J.M., Dice, J.F. and Slaugenhaupt, S.A. (2009) Chaperone-mediated autophagy is defective in mucolipidosis type IV. *J. Cell Physiol.*, **219**, 344–353.
28. Wang, W., Gao, Q., Yang, M., Zhang, X., Yu, L., Lawas, M., Li, X., Bryant-Genevier, M., Southall, N.T., Marugan, J. *et al.* (2015) Up-regulation of lysosomal TRPML1 channels is essential for lysosomal adaptation to nutrient starvation. *Proc. Natl. Acad. Sci. U. S. A.*, **112**, E1373–E1381.
29. Onyenwoke, R.U., Sexton, J.Z., Yan, F., Diaz, M.C., Forsberg, L.J., Major, M.B. and Brenman, J.E. (2015) The mucolipidosis IV Ca^{2+} channel TRPML1 (MCOLN1) is regulated by the TOR kinase. *Biochem. J.*, **470**, 331–342.
30. Curcio-Morelli, C., Charles, F.A., Micsenyi, M.C., Cao, Y., Venugopal, B., Browning, M.F., Dobrenis, K., Cotman, S.L., Walkley, S.U. and Slaugenhaupt, S.A. (2010) Macroautophagy is defective in mucolipin-1-deficient mouse neurons. *Neurobiol. Dis.*, **40**, 370–377.
31. Wong, C.O., Palmieri, M., Li, J., Akhmedov, D., Chao, Y., Broadhead, G.T., Zhu, M.X., Berdeaux, R., Collins, C.A., Sardiello, M. *et al.* (2015) Diminished MTORC1-dependent JNK activation underlies the neurodevelopmental defects associated with lysosomal dysfunction. *Cell Rep.*, **12**, 2009–2020.